UNIVERSIDADE FEDERAL DO RIO GRANDE DO SUL
ESCOLA DE ENGENHARIA - CURSO DE ENGENHARIA MECÂNICA
TRABALHO DE CONCLUSÃO DE CURSO

SOFTWARE IMPLEMENTATION FOR ACOUSTIC EMISSION EVENT DETECTION AND PARAMETER CALCULATION

por

Bernard Claus Obal

Monografia apresentada ao Departamento de Engenharia Mecânica da Escola de Engenharia da Universidade Federal do Rio Grande do Sul, como parte dos requisitos para obtenção do diploma de Engenheiro Mecânico.

Porto Alegre, abril de 2023

CIP - Catalogação na Publicação

Obal, Bernard Claus
SOFTWARE IMPLEMENTATION FOR ACOUSTIC EMISSION EVENT DETECTION AND PARAMETER CALCULATION / Bernard Claus Obal. -- 2023.
15 f.
Orientador: Ignacio Iturrioz.

Coorientador: Boris Nahuel Rojo Tanzi.

Trabalho de conclusão de curso (Graduação) -- Universidade Federal do Rio Grande do Sul, Escola de Engenharia, Curso de Engenharia Mecânica, Porto Alegre, BR-RS, 2023.

1. Acoustic Emission . 2. Automatic event detection. 3. STE-ZCR technique. 4. Python. I. Iturrioz, Ignacio, orient. II. Rojo Tanzi, Boris Nahuel, coorient. III. Título.

Elaborada pelo Sistema de Geração Automática de Ficha Catalográfica da UFRGS com os dados fornecidos pelo(a) autor(a).

Bernard Claus Obal

SOFTWARE IMPLEMENTATION FOR ACOUSTIC EMISSION EVENT DETECTION AND PARAMETER CALCULATION

ESTA MONOGRAFIA FOI JULGADA ADEQUADA COMO PARTE DOS REQUISITOS PARA A OBTENÇÃO DO TÍTULO DE
ENGENHEIRO MECÂNICO
APROVADA EM SUA FORMA FINAL PELA BANCA EXAMINADORA DO CURSO DE ENGENHARIA MECÂNICA

Prof. Cirilo Seppi Bresolin
Coordenador do Curso de Engenharia Mecânica

Área de concentração: Mecânica dos Sólidos

Orientador: Prof. Ignacio Iturrioz

Comissão de Avaliação:

Prof. Ignacio Iturrioz (Presidente)

Prof. Mario Roland Sobczyk Sobrinho

Prof. Tiago Becker

Porto Alegre, 17 de abril de 2023

DEDICATÓRIA

Dedico este trabalho a todos que precisam trabalhar enquanto estudam. A mudança é lenta mas certa, e vale a pena.

AGRADECIMENTOS

Agradeço a minha companheira Gabriela por todo apoio e suporte durante todo o curso de graduação e durante a confecção deste trabalho, sem os quais não teria tido condições de chegar até aqui. Agradeço também o professor Ignacio Iturrioz pelo apoio, e ao colega Boris Nahuel Rojo Tanzi por ter fornecido os dados dos testes e estado sempre aberto a tirar dúvidas.

UNIVERSIDADE FEDERAL DO RIO GRANDE DO SUL
ESCOLA DE ENGENHARIA - CURSO DE ENGENHARIA MECÂNICA
TRABALHO DE CONCLUSÃO DE CURSO – 2023

SOFTWARE IMPLEMENTATION FOR ACOUSTIC EMISSION EVENT DETECTION AND PARAMETER CALCULATION

Obal, Bernard Claus
bernard.claus@gmail.com

Abstract. *This work consists of the development of software that can identify acoustic emission events faster than the acquisition rate, and use them to compute the evolution of local parameters, which can be used as precursors of local and global collapse. The program was developed in Python, using a moving window with a floating threshold in which events are detected using the Short-Term Energy technique. The end is detected using the Zero-Cross-Rate, and is a part of the program that still needs improvement in accuracy. Overall, the program shows good performance and promising results for event detection and parameter calculation.*
Keywords: *Acoustic Emission (AE), automatic event detection, STE-ZCR technique, Python*

NOMENCLATURE

Símbolos

A	Signal amplitude	[V]
E_s	Signal energy	[V s]
f_s	Signal characteristic frequency	[Hz]
t_i	Event start time	[s]
t_f	Event end time	[s]
t_p	Event maximum amplitude time	[s]
A_p	Maximum amplitude value	[V]
Ath	Threshold amplitude value	[V]
RT	Event rise time	[s]
RA	Event rise angle	[s/V]

SUMMARY

1. INTRODUCTION iii
2. THEORETICAL FOUNDATIONS v
2.1 Acoustic Emission Technique (AET) v
2.1.1 b-value v
2.1.2 є-value vi
2.1.3 c-value vi
2.1.4 Average amplitude vii
3. BIBLIOGRAPHICAL REVIEW vii
3.1. Floating threshold for transient AE detection vii
3.2. Short-Term Energy and Zero-Cross Rate (STE-ZCR) analysis viii
4. METHODOLOGY viii
4.1 Event detection ix
4.1.1 Event start detection ix
4.1.2 Event end detection x
5. RESULTS AND APPLICATIONS x
5.1 Results for event detection x
5.2 Application on the spaghetti bridge model xi
5.2.1 Problem description xi
5.2.2 Results xii
5.3 Application on a pre-cracked basalt specimen xiii
5.3.1 Problem description xiv
5.3.2 Results xiv
5.4 Program Graphic User Interface (GUI) xvi
6. RECOMMENDATION FOR FUTURE WORKS xvii
7. CONCLUSION xvii

List of Figures

Figure 1 - Emissions test setup (a) and catalyst efficiency drop after fuel shutoff without further injection (b). Source: (a) https://www.sentronics.com/article/how-temperature-affects-fuel-consumption-measurement-accuracy/ (b) Author. iii
Figure 2 - Configuration of the installed AE sensors in the pillar of the Temple of Athena (a), in the tomato plants stems (b) and in the high-pressure oil pipeline (c), and an AE event example (d). Source: Rojo Tanzi (2020). iv
Figure 3 - Acoustic Emission signal example and the parameters obtained from it. v
Figure 4 - Illustration of the b-value. vi
Figure 5 - Illustration of the RILEM energy (a), the signal RMS (b) and ϵ-value (b). vi
Figure 6 - Illustration of the power spectrum on the frequency domain (a) and c-value (b). vii
Figure 7 - Noise signal in the same test. The variations require a control system to adapt to the noise difference, like the floating threshold. viii
Figure 8 - Two AE events and their duration (green shaded areas) (a), the STE graph for the same time period (b), the STE derivative, in which the first rise will set the event start (c), and the ZCR graph which is used to detect the event ending, by interpreting its decrease when the event start and then its increase as it ends (d). Source: Adapted from Piñal-Moctezuma *et al.* (2019). ix
Figure 9 - Event start detection through STE. x
Figure 10 - Event end detection through ZCR. x
Figure 11 - Results adapted from Rojo Tanzi *et al.* (2021) (a), and each of the parameters obtained with this program (b to h). xiii
Figure 12 - Basalt specimen geometry (a), boundary conditions (b) and photo (c). Source: Rojo Tanzi *et al.* (2022) xiv
Figure 13 - Basalt specimen geometry load applied (a) and event count (b). xiv
Figure 14 - Results for b-value adapted from Rojo Tanzi *et al.* (2022) (a), results from this program (b). xv
Figure 15 - Results for ϵ-value adapted from Rojo Tanzi *et al.* (2022) (a), results from this program (b). xv
Figure 16 - Results for c-value adapted from Rojo Tanzi et al. (2022) (a), results from this program (b). xvi
Figure 17 - Results for the average amplitude. xvi

1. INTRODUCTION

The large amount of available information nowadays makes data treatment and analysis one of the most important tools in decision-making in a variety of fields ranging from biology and marketing, social networks and engineering. The technologies developed around data analysis continuously increase their influence over our daily lives. One example we could mention is the analysis of certain vehicle parameters, such as air-fuel mixture enrichment after a fuel shutoff event not followed by acceleration, in order to increase catalyst efficiency, thus reducing pollutants emissions (Choi *et al.*, 2019), an effect illustrated in Figure 1b. Another example that can be mentioned is the combined analysis of data collected from a hospital to improve its efficiency (Kohl *et al.*, 2019), and even the usage of user access data from a social network to determine the best time for posting new content in order to get more viewers.

Figure 1 - Emissions test setup **(a)** and catalyst efficiency drop after fuel shutoff without further injection **(b)**. Source: (a) https://www.sentronics.com/article/how-temperature-affects-fuel-consumption-measurement-accuracy/ (b) Author.

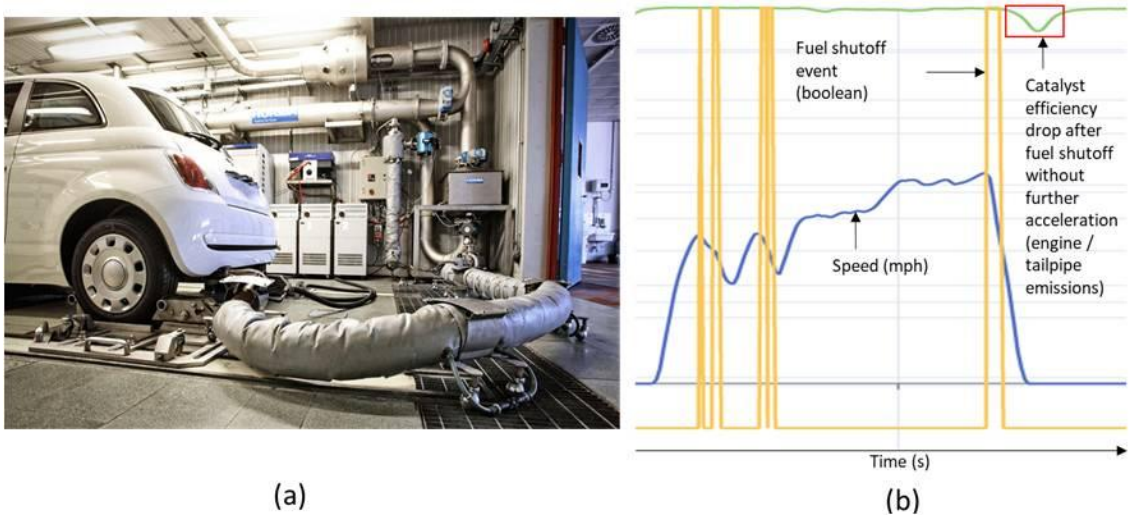

In engineering, damage determination and measurement using the structure response are widely used in maintenance and monitoring of structures of great interest, such as oil pipelines, old buildings, among others. Among these data analysis techniques, one that stands out is the acoustic emission technique (AET), which consists of obtaining characteristic signals caused by elastic waves generated by internal mechanisms in the system. AET can be used in non-destructive tests, with real-time analysis while the system conditions continuously change, for example when applying load to a structure, increasing internal pressure of a pipeline or the growth process of a plant, which makes this technique very valuable in the monitoring of systems whose conditions change over time. Three usage examples of AET are: the monitoring of a 2500-year-old structure in Italy called Temple of Athena, whose pillars are excited by the weight of structure itself and by the surrounding traffic of vehicles and people (Figure 1a), mentioned by Carpinteri *et al.* (2008a); the monitoring of a tomato plant growth, in order to establish the best irrigation regime (Figure 1b), mentioned by Kageyama and Sakai (2016); the monitoring of high pressure oil pipelines (Figure 1c), mentioned by Quo *et al.* (2020).

Figure 2 - Configuration of the installed AE sensors in the pillar of the Temple of Athena (a), in the tomato plants stems (b) and in the high-pressure oil pipeline (c), and an AE event example (d). Source: Rojo Tanzi (2020).

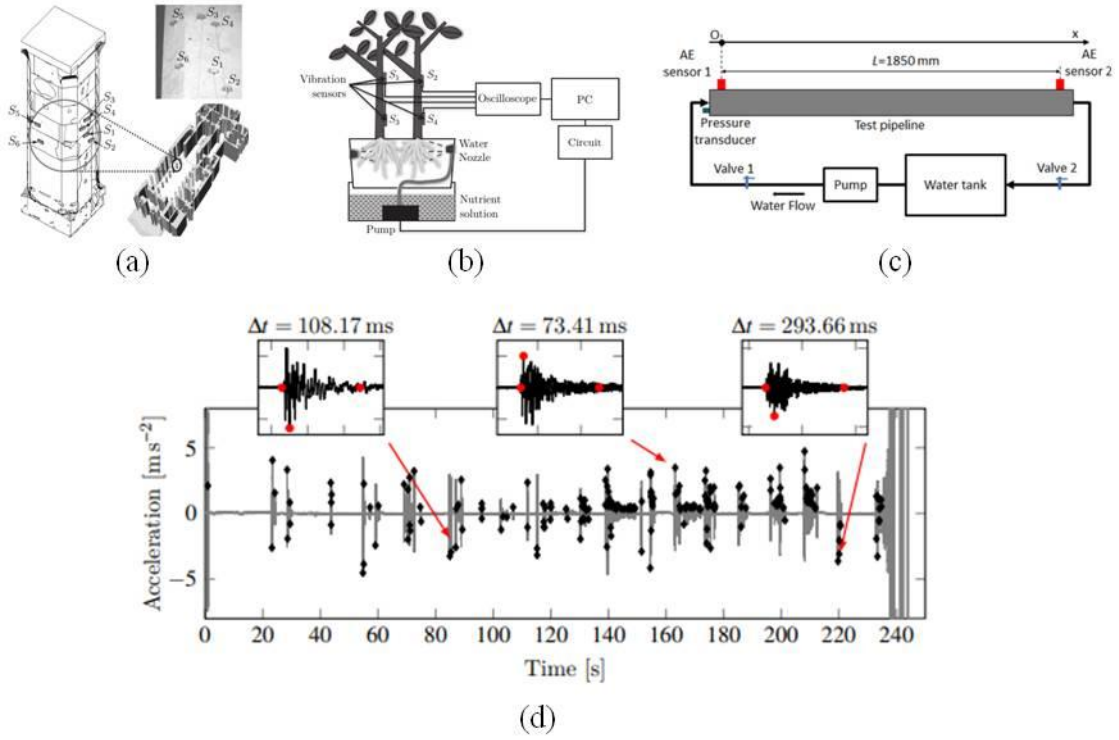

Through the identification of acoustic emission (AE) signals, it's possible to compute global parameters, and the evaluation of their evolution can indicate a change in the system conditions, for example, that a structure is about to collapse. In this context, it is possible to define the general objective of this work, which is to develop a tool for AE studies capable of interpreting data faster than the acquisition rate. The specific objectives are the following:

- Apply array programming techniques to speed up event detection, as described by Harris *et al.* (2020);
- Calculate the evolution of global parameters used in the Acoustic Emission Technique;
- Validate the program by comparing its results to other results obtained with the same dataset;
- Discuss the damage process identification by analyzing the graphic of the parameters.

Structure of this paper

Section 2 presents the theoretical foundations that describe the physical meaning of the events and obtained parameters, along with the techniques used for obtaining them. Section 3 contains a bibliographical review of tested AE event detection techniques. Section 4 contains the results obtained from this program, and shows the graphic with all the values of the parameters obtained in the validation process. Section 5 is the conclusion, where we discuss the obtained values.

2. THEORETICAL FOUNDATIONS

2.1 Acoustic Emission Technique (AET)

This technique consists of mounting Acoustic Emission (AE) sensors on the system surface, from which data is collected and can either be stored for future analysis or be used to monitor structures in use (such as a pressure vessel). These sensors are capable of detecting the elastic waves that propagate in the solid, as a result of changes in its internal structure. According to Ohtsu (2015), "*Fracture in a material takes place with the release of stored strain energy, which is consumed by nucleating new external surfaces (cracks) and emitting elastic waves*". The sensors measure acceleration of high frequency, normally ranging from 20 kHz to several MHz, according to Grosse and Ohtsu (2008). Figure 3 illustrates a typical Acoustic Emission signal where one event has occurred, and some parameters extracted from this event. These are individual parameters, and combined, they generate some indicators of system collapse, as described by Ohtsu (2015).

Figure 3 - Acoustic Emission signal example and the parameters obtained from it.

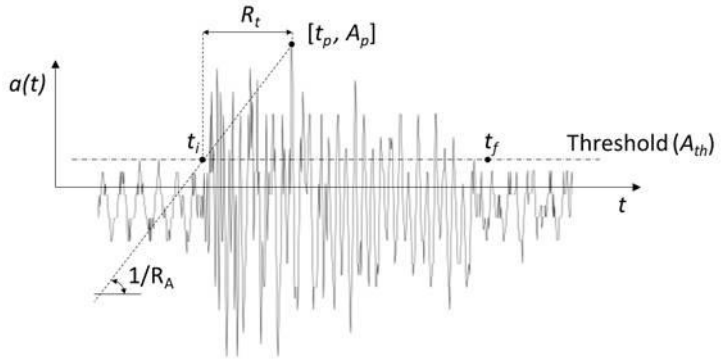

The forementioned parameters include the event start time (t_i), end time (t_f), and moment of maximum amplitude (t_p), maximum amplitude value (A_p), threshold amplitude value (A_{th}), rise time ($RT = t_p - t_i$), and rise angle ($RA = RT / A_p$).

2.1.1 b-value

The b-value, or Gutenberg–Richter coefficient, was first introduced in the evaluation of seismic events in the 1940s. It defines a relationship between the number of events (N) and their amplitude (A). First, we count the number of events with amplitude equal or greater to the amplitude of each point, in a moving window containing a defined amount of events, and then make a linear regression of these points in a bi-log graph of number of events and amplitude, as illustrated in Figure 4. The b-value represents the angular coefficient of this regression, according to Eq. 1.

$$N(\geq A) \propto A^{-b} \qquad \text{(Eq.1)}$$

Figure 4 - Illustration of the b-value.

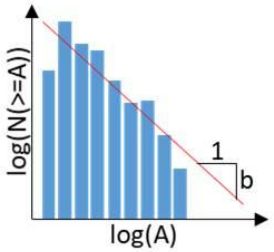

When the damage process starts in a structure, the events originate from small micro-cracks and are of lower amplitude and more homogeneously distributed, which results in a high b-value. As damage progresses, the micro-cracks generate events with a larger amplitude that tend to accumulate in a preferential place, which in turn reduces the number of events larger than those amplitudes, reducing the b-value.

2.1.2 ϵ-value

This value is computed in a similar way to the b-value, but relates energy of the signal (Es) to the number of events, as in Eq. 2.

$$N(\geq E_s) \propto {E_s}^{-\epsilon} \quad \text{(Eq.2)}$$

The energy can be obtained by the RILEM method, which consists of calculating the area of a triangle made of the start point, end point, and peak amplitude point of the signal – RILEM Technical Committee (Masayasu Ohtsu), 2010 - or by simple RMS value of the signal. Using the RMS signal has yielded improved sensitivity compared to the RILEM method, as observed by Rojo Tanzi *et al.* (2021). Both are used in the program. Figure 5 (c) illustrates the calculation of the ϵ-value.

Figure 5 - Illustration of the RILEM energy (a), the signal RMS (b) and ϵ-value (b).

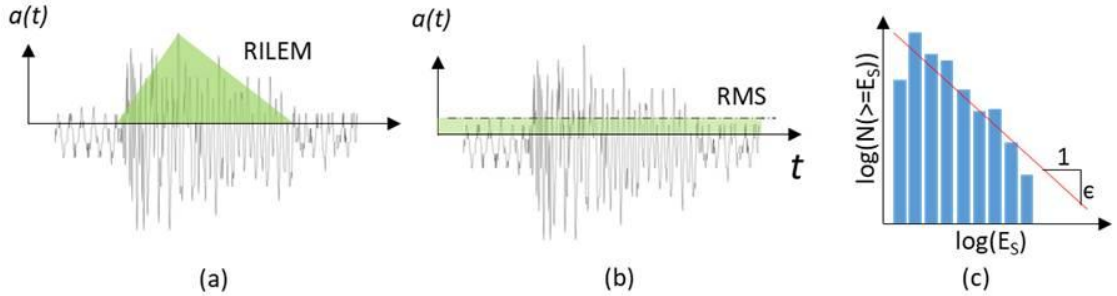

2.1.3 c-value

The calculation of this parameter is similar to that of values b and ϵ, and it focuses on the frequency distribution of the AE events, related to the number of events, as in Eq. 3.

$$N(\geq f_s) \propto {f_s}^{-c} \quad \text{(Eq.3)}$$

For each event, a Fast Fourier Transform is applied to the signal, and the frequency with the largest power spectral density is considered the characteristic frequency of that event. While the damage process changes and the micro-cracks start to grow, the c-value decreases, indicating an imminent collapse of the structure. Figure 6 shows an illustration for obtaining the c-value.

Figure 6 - Illustration of the power spectrum on the frequency domain **(a)** and c-value **(b).**

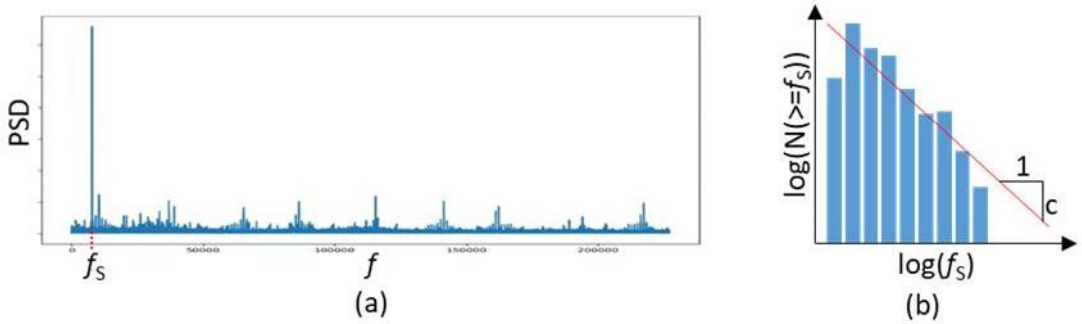

2.1.4 Average amplitude

The average amplitude is the simple average of the amplitude values from the events inside the moving window. It is reported by Belousova and Grigorieva (2018) that it helps track the dynamics of crack formation. This parameter is complementary to the b-value.

3. BIBLIOGRAPHICAL REVIEW

In this section, we review the event detection techniques used in previous works. Event detection is a basic functionality to find where each event starts and ends, in order to obtain the event parameters shown in Figure 3, and it is discussed in several papers. The most basic technique is setting a fixed amplitude threshold above which the signal is considered an event. However, this can lead to imprecise detection of AE events, especially when the noise floor amplitude has significant variations. Therefore, more precise techniques were developed, two of them are explained in the next section, one by Xiang (2017) and another by Piñal-Moctezuma, F. et al. (2019).

3.1. Floating threshold for transient AE detection

There are many solutions for AE event detection, some of which require much processing time and are not suitable for processing data faster than the acquisition rate. The threshold is the simplest and most used way of locating the AE signals, however, when the noise amplitude presents variations, as illustrated in Figure 7, a single threshold fails to correctly identify the events, returning too many false positives or not locating an event, if it was set too low or too high. One workaround for that problem, mentioned by Xiang (2017), is to recalculate the threshold in a moving window, which sets a higher threshold for noises with more amplitude. The author suggests making the signal envelope, calculating the mean of the envelope, and then setting the threshold to three times the standard deviation of the envelope above the mean. To be considered AE

events, only points that have consecutive spikes above the threshold are considered possible AE events, which rules out outliers.

Figure 7 - Noise signal in the same test. The variations require a control system to adapt to the noise difference, like the floating threshold.

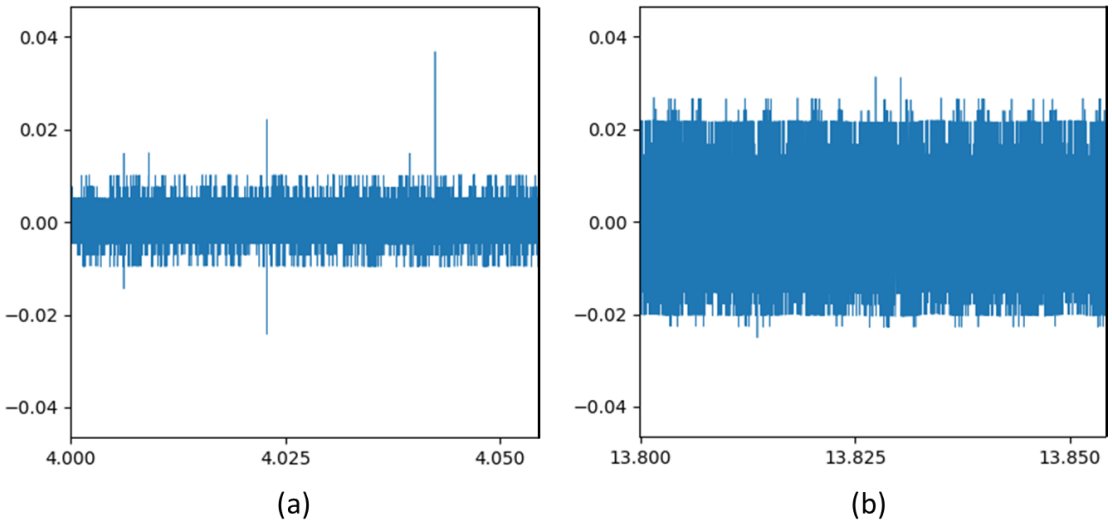

3.2. Short-Term Energy and Zero-Cross Rate (STE-ZCR) analysis

This technique is mentioned by Piñal-Moctezuma et al. (2019), and detects events through a refined multi-step technique. The first step is the generation of characteristic functions for the short-term-energy (STE), which is the sum of the square of each point's absolute value, and the zero-cross-rate (ZCR), which is the time it takes for the signal to change its sign from negative to positive or vice-versa. Then the event start points are determined by the positive derivative STE signal, and the endpoints of the events are determined by the rise of the ZCR derivative. This is due to the events having greater energy than the noise signal, and also having a much smaller ZCR than the noise signal. The combination of both values makes a reliable indicator of the event duration. The result of this technique is illustrated in Figure 8, where in (a) we see the event signal highlighted from start to finish. On (b) we see the STE value used to detect that an event is happening, on (c) we see the STE derivative, used to find the event start time, and on (d), we see the ZCR derivative, where the leftmost yellow highlighted square, as well as the third square, highlighted in blue, are used to set the threshold to which the signal must return in order for next the event to end.

4. METHODOLOGY

In this work, data was acquired from tests performed at the GMAp (Grupo de Mecânica Aplicada – Applied Mechanics Group) at UFRGS, and are used as input for the program, which runs simulations on acquired data. The data for both tests was supplied by GMAp, and the papers they relate to are Rojo Tanzi et al. (2021) and Rojo Tanzi et al. (2020).

The code development is made with Python language – reference to Ernesti, J., Kaiser, P (2022) - with the assistance of the mathematical library NumPy. User interface is made with built-in library tkinter and matplotlib for the graphs.

Figure 8 - Two AE events and their duration (green shaded areas) **(a)**, the STE graph for the same time period **(b)**, the STE derivative, in which the first rise will set the event start **(c)**, and the ZCR graph which is used to detect the event ending, by interpreting its decrease when the event start and then its increase as it ends **(d).** Source: Adapted from Piñal-Moctezuma *et al.* (2019).

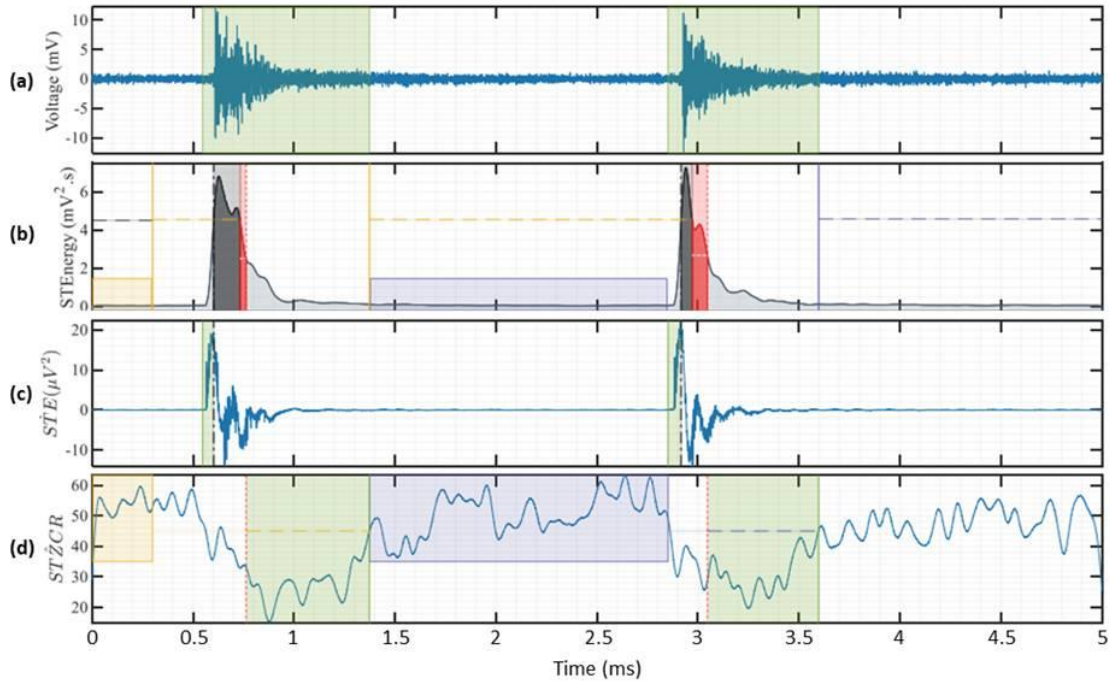

4.1 Event detection

In order to obtain the indicators that assist the user in identify significant damage to the analyzed structure, first the parameters of each event must be obtained, and the first part is to identify the event start and end times. Within this time, we obtain the maximum amplitude, energy and characteristic frequency.

The detection is made within each moving window, which have their own amplitude threshold set based on the specific window noise, as described in Section 3.1. Points above this threshold are separated for further analysis. The procedure is first to create a top envelope of the signal (which reduces the number of points and facilitates analysis), then setting the threshold to three times the standard deviation above the mean value of the envelope, as suggested by Xiang (2017). This multiplier of three times is adjustable by the user to increase or reduce sensitivity.

After setting the threshold for the window, all the envelope points above it are analyzed with 2 parameters: the Short-Term Energy (STE) and the (ZCR). This technique is described in Section 3.2.

4.1.1 Event start detection

The STE is used to detect the event start. The algorithm finds the points where the envelope crosses the threshold, then for a set number of following neighbors, set to 10 as the standard but configurable by the user, it checks if there are at least 2 other points above the threshold that are in a row or with one gap between them. If there are, it

calculates the total energy of this segment, and if not, it gives a value of zero. This filters out false positives, and the event start is identified where the energy goes above zero, as illustrated in Figure 9.

Figure 9 - Event start detection through STE.

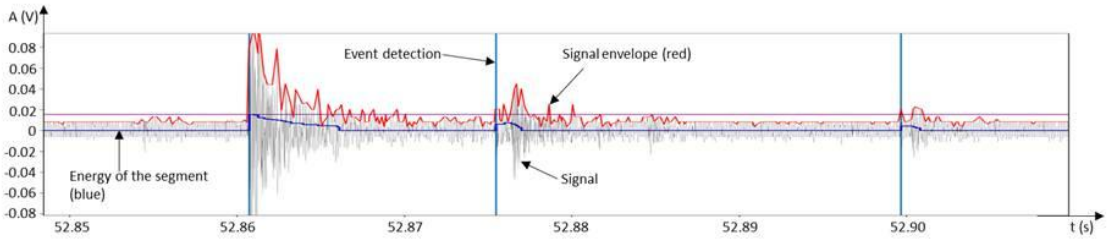

4.1.2 Event end detection

The end is detected via the ZCR where the Nth point after an event starts that passes the ZCR envelope average. N is defined by the user and is set by default to 5 to avoid early detection by noise. Figure 10 illustrates in blue the event start, detected via STE, the ZCR in green, the ZCR envelope average in a red horizontal line, and the event end, represented by vertical red lines. The event duration is represented by the painted rectangles.

Figure 10 - Event end detection through ZCR.

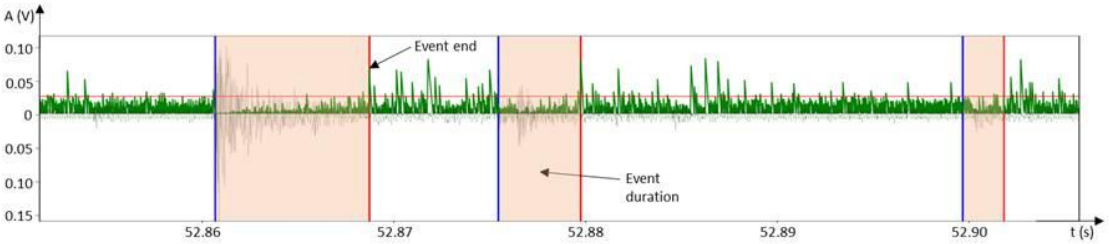

5. RESULTS AND APPLICATIONS

In this section, we test this algorithm with two acoustic emissions signals that have already been interpreted and have had their results published in papers and compare the results for the indicators to check the program's accuracy. The event detection quality is discussed in section 5.1.

5.1 Results for event detection

The most important part of the program is the automatic event detection, and that includes obtaining its start and end points, which can affect mostly the ϵ and c values, since the b-value and the average amplitude use only the event amplitude as input. The event detection part of the algorithm has indicated that it works well in detecting an event start and its highest amplitude, but is not very precise in detecting the event end, mainly due to the ZCR average being affected by a long signal (in relation to the window size) of great amplitude, which sets the window average to a lower value. This causes the threshold to be lower, and small noises already pass the average, causing an early event end detection. In some cases, when the event has a length that is short in relation to the window (0.05), then the detection works well. In cases where the event

has a length of 0.15, three-quarters of the window size, the event is split into parts, and 4 events were detected in this specific case.

Furthermore, in windows where the signal was mainly noise, some false detections of long but small amplitude events happened. An example of this is illustrated in Figure 11c.

These detection errors are a common problem in automatic event detection algorithms, as mentioned by Xiang (2017) - "*[...] when the noise floor amplitude has significant change, an appropriate threshold is not easy to be obtained to trigger the AE signal alarm."*

5.2 Application on the spaghetti bridge model

This AE signal originated from a spaghetti bridge competition held at the Federal University of Rio Grande do Sul (UFRGS) by mechanical engineering graduation students, and its results were the subject of the paper by Rojo Tanzi *et al.* (2021).

5.2.1 Problem description

The bridge studied in the paper is supported on both sides, and the load is applied at the bottom center point. One AE sensor is installed on the side and the other at the top of the bridge. Four pictures of the experiment at different times during the test are shown on Figure 11, and the sensors are pointed out on Figure 11a.

Figure 11 - Spaghetti bridge model at various moments during the test. Source: Rojo Tanzi et al. (2021).

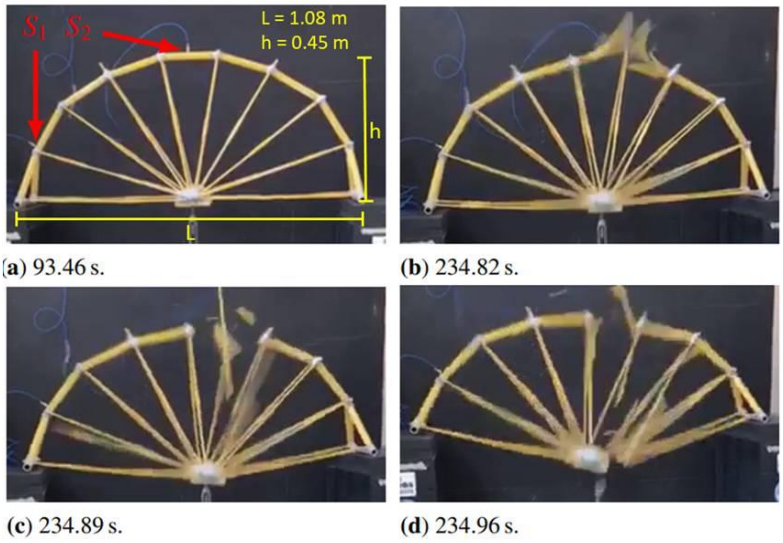

The bridge is 1.08 m long, 0.45 m high, and 0.15 m wide, with a mass of 1.40 kg. The load is increased every 10 s and the bridge collapsed with a load of 784.80 N at 235 s into the test. According to the author Rojo Tanzi (2021), "*the sensors are piezoelectric accelerometers, with frequency measurement in lineal range from 5 Hz to 60 kHz. Their signal was acquired through a data acquisition module Brüel & Kjær® PULSE™ 3035, at a sampling rate of 65.54 kHz. A Nyquist-type filter with a cutoff frequency of 30 kHz was used in order to reduce noise and to avoid aliasing*". The data was processed using the SoftAE software, whose creation was part of the dissertation by Rojo Tanzi (2020).

5.2.2 Results

The test results obtained with this algorithm are presented on Figure 12 (b to h) along with the results previously obtained by Rojo Tanzi et al. (2021) on (a), which displays all parameters (b-value, c-value, ϵ value for frequencies using RMS and RILEM, and event count). Each indicator is individually evaluated in the next sections. The histograms for b-value, ϵ-value and c-value are made with 25 events with 5 events overlap, the same as in the previous study. This program has found 445 events, as opposed to 230 events found in the previous program, mainly because of the event end detection described in Section 5.1, which led to many events being split in more than one part.

(a) b-value: The b-value illustrated on Figure 11b presents instabilities in the regions between 120 s and 150 s, with peaks on 123.63 s, 134.54 s and 146.23 s, while the load increases occurred at 117.88 s, 131.34 s and 142.88 s. This shows that this indicator responds to the load variation, which can also be noticed in the graph for the ϵ-value Figure 11c. Overall, the b-values obtained correlate well with the ones already studied, and the load characteristics of the test, which shows that the program worked well on obtaining this parameter.

(b) ϵ-value: The ϵ-value results are illustrated on Figure 11d, and show a significant change around the 150 s mark, which represents a likely change in the system characteristics. This behavior is also seen on the previous study on Figure 12a.

(c) c-value: The c-value is the parameter with the biggest difference from the previous study. It shows a slight decrease between 135 s and 140 s, but the magnitude of the decrease is small and not very conclusive. This difference is likely related to the software difficulty in finding the correct event endpoint, and since this parameter is affected by the event length as the frequency decays throughout the event, the differences can be significant. To improve that, more work must be done in correcting the event end detection.

(d) Average amplitude: This parameter was not registered in the previous study, but was inserted in the program due to its possible relevance, as mentioned in section 2.1.4. The average amplitude has shown a big increase between 140 s and 150 s, along with the other noticeable changes in the other parameters, and another at the end of the test after 210 s, and finally a major one at 234 s. This was the only parameter to show a good response at the end of the test (after 210 s) near the collapse, which points to its importance in structural monitoring.

Figure 11 - Results adapted from Rojo Tanzi *et al.* (2021) **(a)**, and each of the parameters obtained with this program **(b to h).**

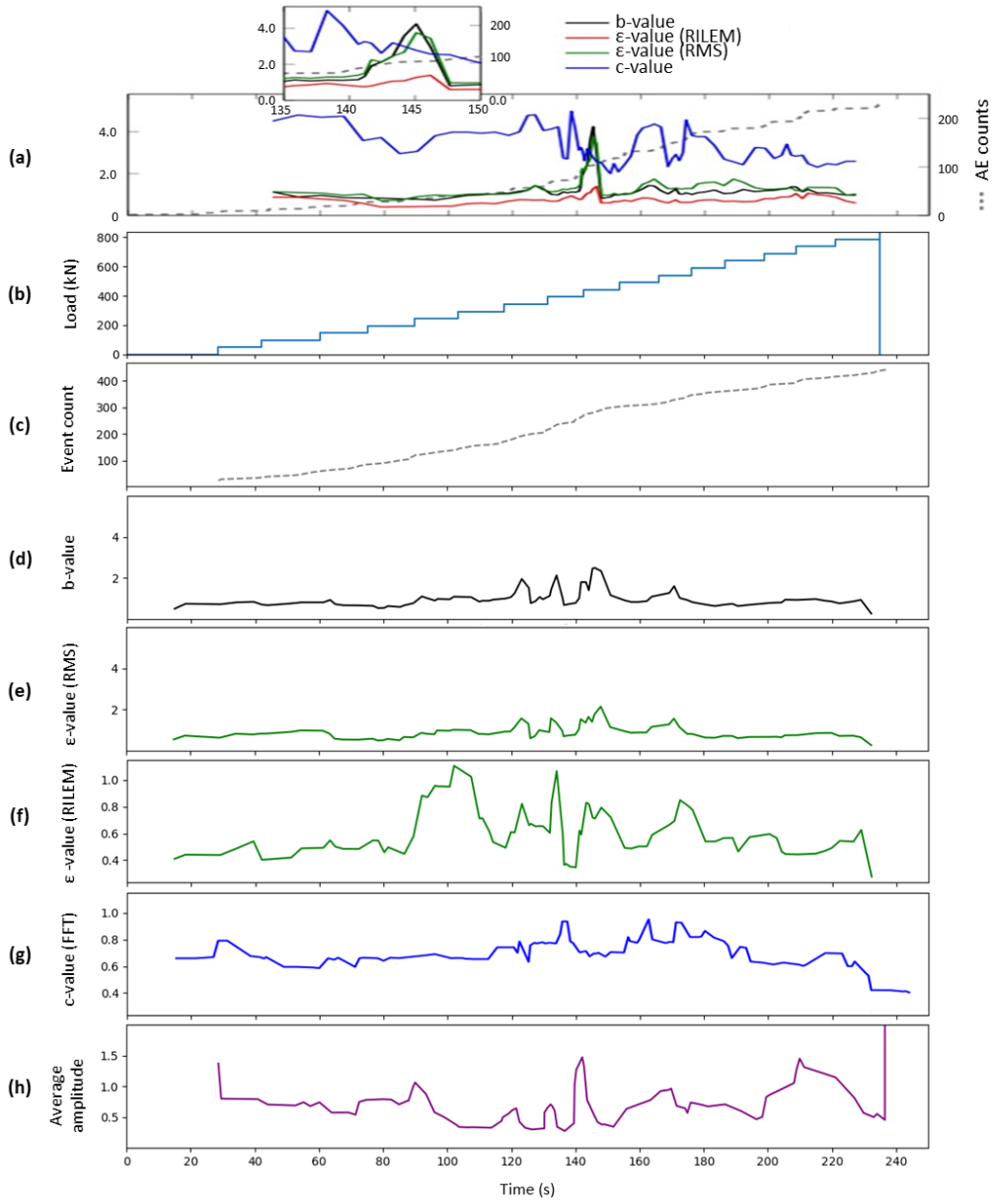

5.3 Application on a pre-cracked basalt specimen

This AE signal originated from a test in a prismatic basalt specimen with an oblique pre-fissure, and its dimensions, boundary conditions, and photo are shown in Figure 12, and it was first analyzed by Rojo Tanzi *et al.* (2022).

Figure 12 - Basalt specimen geometry (a), boundary conditions (b) and photo (c). Source: Rojo Tanzi *et al.* (2022).

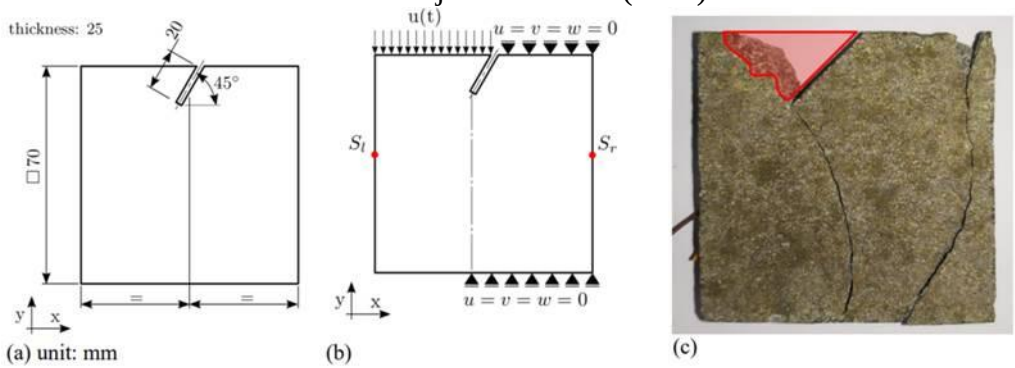

5.3.1 Problem description

The measurements were performed with a data acquisition system with a frequency of 445 kHz, with two sensors, one on each side of the specimen, and the prescribed displacement was applied at a constant velocity of 0.6 mm/min. The specimen is a square with 70 mm sides and 25 mm thickness.

5.3.2 Results

The test results obtained with this algorithm are presented on the result section for each parameter, along with the results previously obtained by Rojo Tanzi *et al.* (2022). The load and event count are displayed on Figure 13. Each indicator is individually evaluated in the next sections. The histograms for b-value, ϵ-value and c-value are made with 35 events with 3 events overlap, the same used on the previous study. This program has found 1289 events, as opposed to 1274 events found in the previous program. A manual review of the data indicated 211 false positive detections, 16%.

Figure 13 - Basalt specimen geometry load applied **(a)** and event count **(b).**

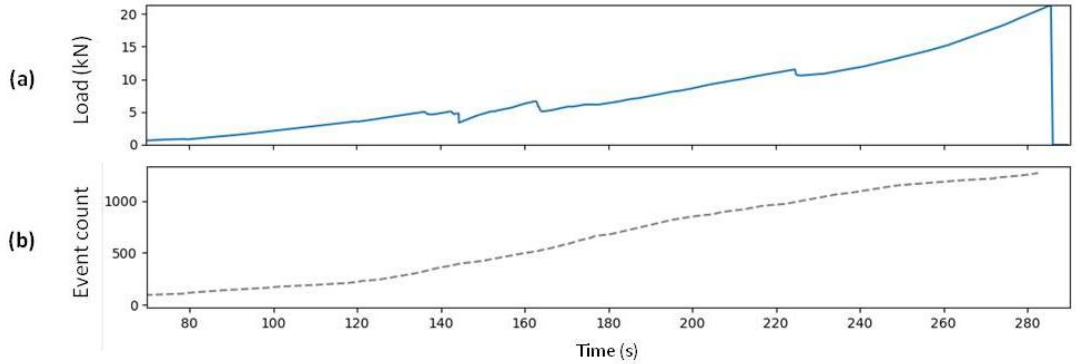

(a) b-value: The b-values obtained are illustrated on the graph in Figure 14, where (a) is the result from the previous study and (b) from this program. The graph shows a steep decrease in the b-value at 107 s, and in the previous study there is one at 114 s (marked as point (a)), and this delay is linked to the event detection. Since the windows are calculated for every three new events, if a false event is identified, then a b value will be generated in advance. If, on the other hand, an event is overlooked, then this will lead to a delay in the generation of the next value. Moreover, we see low points of b-value in the ranges of 125 s to 135 s and also between 135 s to 145 s, observable in both

graphs. The third critical point is the steep decrease near 220 s, where the b-value drops below 1, and the fourth is the drop at 275 s. The overall comparison of both results shows a good connection between the obtained b-values and the test critical points.

Figure 14 - Results for b-value adapted from Rojo Tanzi *et al.* (2022) **(a)**, results from this program **(b).**

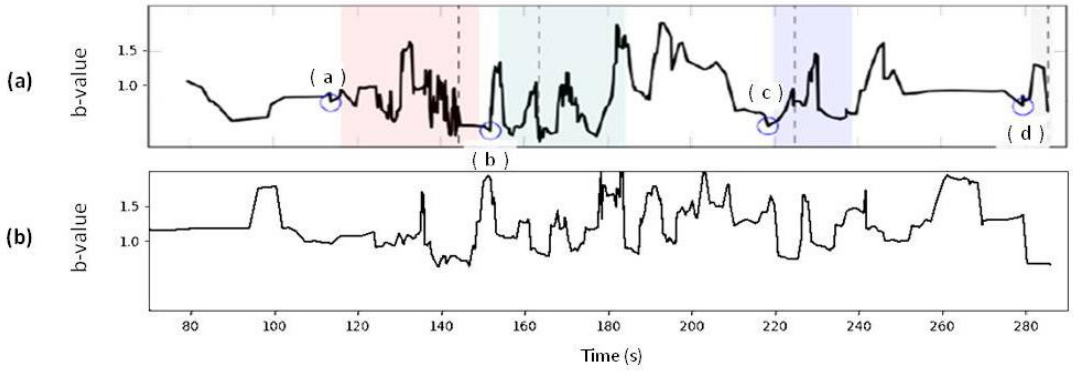

(b) ϵ-value The ϵ-values graph is on Figure 15, where (a) is from the previous study, (b) is the value obtained using the signal RMS, and (c) is the value obtained using the RILEM method. The results from this program show steep decreases in ϵ at around 120 s, where it goes just below 1, and a sudden increase at 130 s, behavior also observed in the previous study between 125 s and 131 s. The next point of interest is another valley with steep edges between 135 s and 151 s, where c again drops below 1, The next sudden changes happen between 220 s and 227 s. The results obtained using the RILEM method had much smaller amplitudes overall and displayed only three steep changes at 146 s, 204 s, and two smaller ones at 220 s and 268 s. These decreases to low values coincide with the times where critical events occurred. The low amplitude and small variation of this parameter with RILEM reflect the event identification problem.

Figure 15 - Results for ϵ-value adapted from Rojo Tanzi *et al.* (2022) **(a)**, results from this program **(b).**

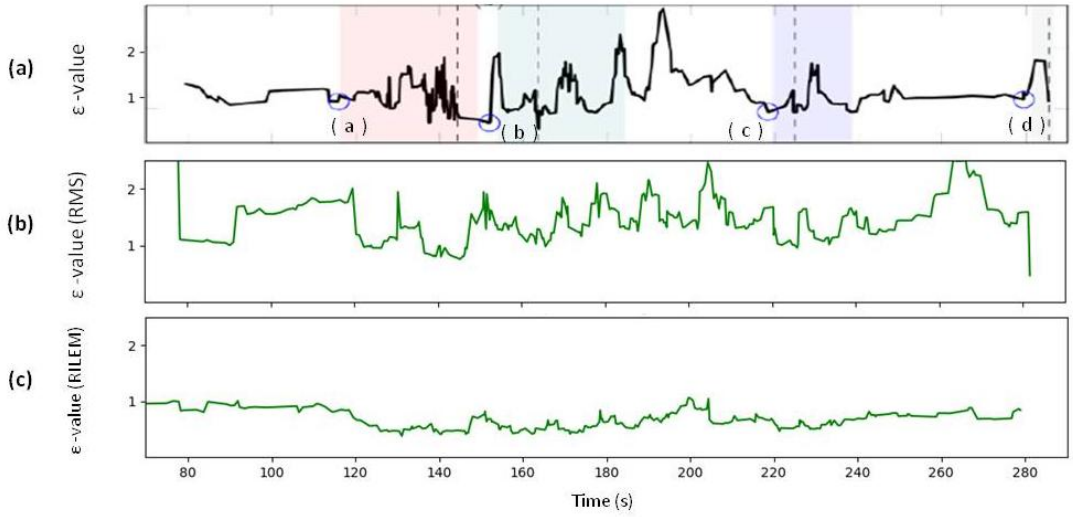

(c) c-value: The c-values obtained show the same rapid decrement behavior as the previous study results at 145 s, 158 s and 180 s. These rapid drops in the c value

indicate a change in the system configuration. The plot for these values is illustrated in Figure 16.

Figure 16 - Results for c-value adapted from Rojo Tanzi et al. (2022) **(a)**, results from this program **(b).**

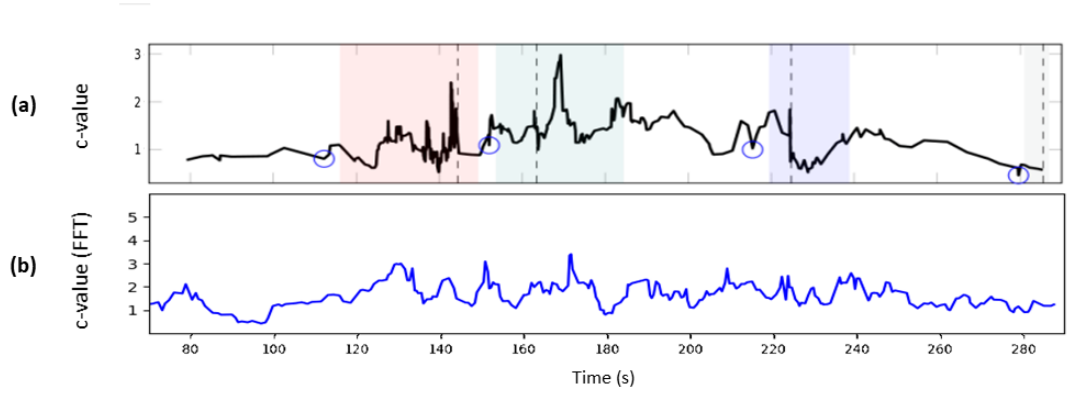

(d) Average amplitude: Again, the average amplitude demonstrated to be a good indicator of relevant changes happening in the system characteristics. It shows a very large increase in the two first critical areas, and a noticeable spike on the third one, and the variations are very clear due to their amplitude. This parameter was not obtained for the previous paper, so we can only compare this parameter's behavior against the critical zones. Its illustration is on Figure 17.

Figure 17 - Results for the average amplitude.

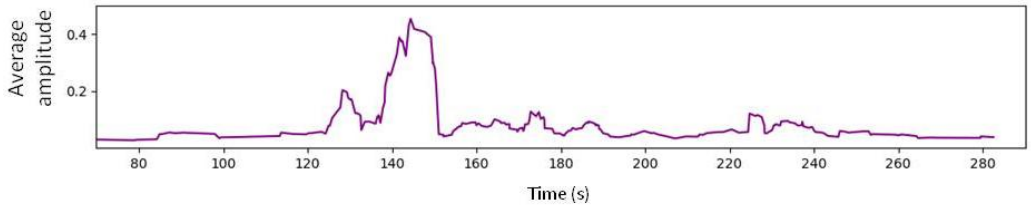

5.4 Program Graphic User Interface (GUI)

The GUI main window, seen on Appendix I – Fig. 1, consists of a graphic that displays the live signal on the top, along with the events found highlighted in green. The user has the option to pause the visualization (which does not pause the acquisition and processing of data), shift the view back and forth, and return to live to see the most recent data. The events are all stored and the user can visualize a list of events, shown in Appendix I – Fig. 2, and select an event to view in a separate window, as observed in Appendix I – Fig. 3. On the main window, there are also graphics for each parameter, also generated live (these do not pause). The program generates a report in CSV containing all the event parameters, and all the event plots are recorded in a PDF file, one event per page, as shown in Appendix II. This allows quick testing using different input configurations, which can speed up the analysis and save important engineering time.

6. RECOMMENDATION FOR FUTURE WORKS

The most significant part of the program is the event detection, from which all the other parameters are calculated. Therefore, efforts in the direction of improving event end detection despite the window size and noise are interesting. One unsuccessful attempt involved making a linear regression of the event signal envelope and using it for end detection when it crossed zero, but the events are very unpredictable at the start and when there are ‘s’ waves for example, which increase in amplitude slowly, the first part of the event may have positive derivative. Other improvements to this program is code review to optimize performance, and study the relation between the signal characteristics and the parameters obtained to add calibration to a control system acting on the ZCR threshold, in order to improve event end detection.

7. CONCLUSION

The objective of creating a software with a graphic user interface, capable of interpreting an AE signal, identifying events, and generating local parameters on data obtained in buffers was successfully achieved. The analysis using a moving window with a floating threshold works well in most cases, but has limitations when the whole window has only noise and therefore a small standard deviation, which triggers long, false events. When the event length is close to the size of the window, it lowers the ZCR average and leads to the detection of many events with a short duration. The ZCR derivative has a noticeable decrease when an event starts, but finding a threshold above which the end is correctly detected is not easy because of the same limitations of the floating threshold mentioned earlier. The STE analysis for event start detection works well overall, detecting precisely the start of most events. The average amplitude demonstrated to be a good precursor of failure, as it increases near the critical points. The calculated values for b, ϵ, c and the average amplitude showed a good response to the tests critical points where the system suffered a configuration change. In the case of the Spaghetti bridge model, that had the load in a step pattern, coincided with the load increases, which points to a good relationship between the program output and the real event. For future works, it is suggested to improve end time detect precision. Overall, the program created provides fast response in a graphic user interface (illustrated in Appendixes I and II) and reports in CSV and PDF format, allowing quick tests using different input configurations, which can speed up the analysis and save important engineering time.

REFERENCES

BELOUSOVA, V.; GRIGORIEVA, A. Development of a software package for acoustic emission control data analysis, Saint Petersburg State University, p. 6, 2018.

CARPINTERI, A.; LACIDOGNA, G.; INVERNIZZI, S.; MANUELLO, A.; BINDA, L. Stability of the vertical bearing structures of the Syracuse Cathedral: experimental and numerical evaluation, Materials and Structures, vol. 42(7), p. 877, 2008.

Choi, M.; Song, J.; Lee, E.; Ma, S. The Development of a NOx Reduction System during the Fuel Cut Period for Gasoline Vehicles. SAE Technical Paper. 2019-01-1292, p. 1, 2019.

ERNESTI, J., KAISER, P., Python 3 – The comprehensive guide, Rheinwerk, 2022.

GROSSE, C. U.; OHTSU, M. Acoustic Emission Testing, Ed. Springer: Berlin/Heidelberg, Germany, p. 406, 2008.

HARRIS, C. R., *et al*, Array programming with NumPy, pg. 1, 2020.

KAGEYAMA, K.; SAKAI, T., Evaluation of Irrigation Response using AE Method for Management of High-Frequency Irrigation of Hydroponic Miniature-Tomato, Journal of Acoustic Emission, vol. 34, p. 65–70, 2016.

Kohl, S.; Schoenfelder, J.; Fgener, A.; Brunner, J. The use of Data Envelopment Analysis (DEA) in healthcare with a focus on hospitals, p. 1, 2019.

OHTSU, M., Acoustic Emission (AE) and Related Non-destructive Evaluation (NDE) Techniques in the Fracture Mechanics of Concrete, Kumamoto University, Kumamoto, Japan, p. 1, 2015.

PIÑAL-MOCTEZUMA, F.; DELGADO-PRIETO, M.; ROMERAL-MARTÍNEZ, L. An Acoustic Emission Activity Detection Method based on Short-Term Waveform Features: Application to Metallic Components under Uniaxial Tensile Test, pg. 4-14, 2019.

PRABHAT, R. P. *et. al*. Damage characterization of reinforced concrete beams under different failure modes using acoustic emission, CSIR-Structural Engineering Research Centre, India, p. 14, 2021.

QUY, T.B. *et. al.* Crack detection and localization in a fluid pipeline based on acoustic emission signals, p. 1, 2020.

RILEM, T. C. Recommendation of RILEM TC 212-ACD: acoustic emission and related NDE techniques for crack detection and damage evaluation in concrete: Measurement method for acoustic emission signals in concrete. Materials and Structures, vol. 43(9), p. 1177-1181, 2010.

ROJO TANZI, B. *et. al*. Damage Evolution Analysis in a “Spaghetti” Bridge Model Using the Acoustic Emission Technique, UFRGS, p. 9, 2021.

ROJO TANZI, B. Análise do processo de dano com a técnica de emissão acústica e métodos discretos, UFRGS, p. 14-15, 2020.

ROJO TANZI, B. *et al*. The damage evolution in specimens made with quasi-brittle materials: Experimental verification using Acoustic Emission technics, UFRGS, p. 4, 5, 2022.

XIANG, D. Acoustic Emission Detection of Early Stages of Cracks in Rotating Gearbox Components, X-wave Innovations, p. 7, 2017.

APPENDIX I – Program GUI

Figure 1 – Program GUI main window. On the top is the live signal, and the others are the evolution of the calculated parameters in time

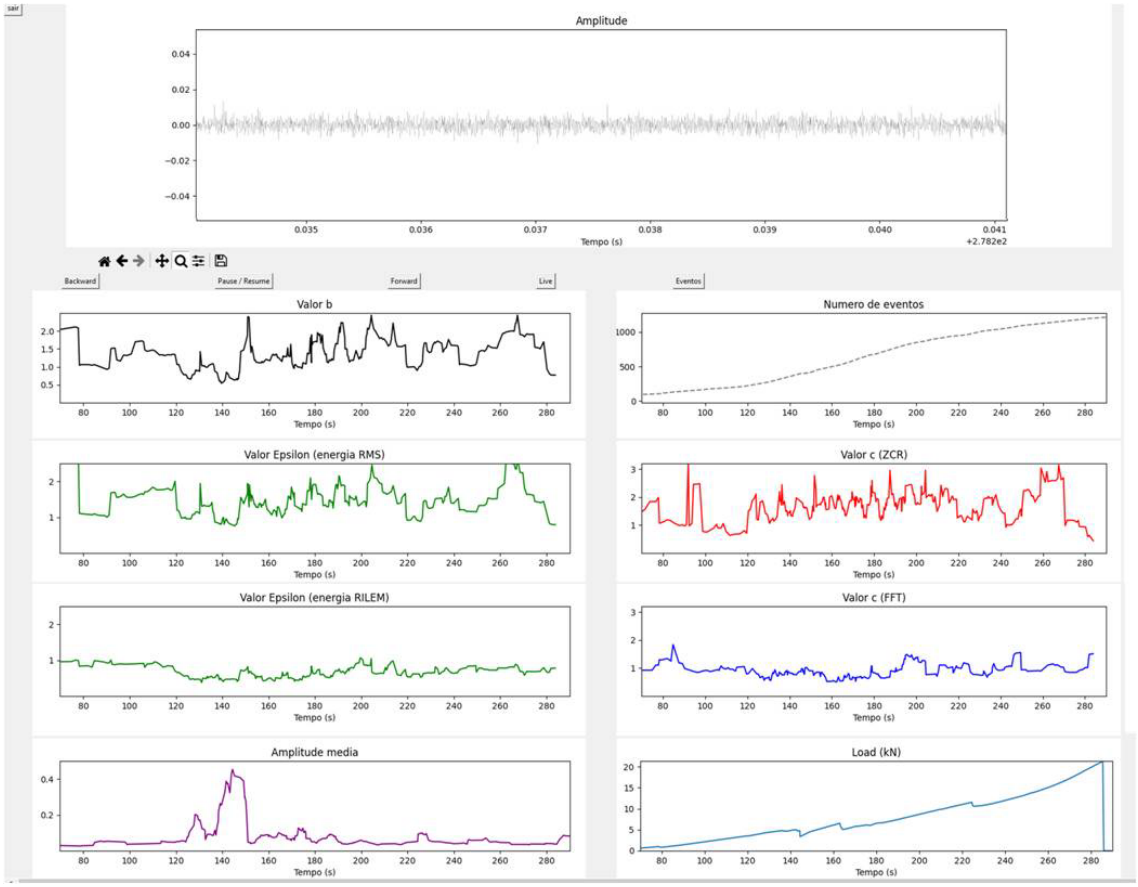

Figure 2 – Program GUI events window

sair — Para visualizar um evento, clique em "Ver"

#	Inicio	Fim	Duracao	Energia RILEM	Energia RMS	Amplitude	Freq FFT	Freq ZCR	Visualizar
1	0.8837890625	0.9008331298828125	0.0170440673828125	0.07360265629730095	2.377437962354066	8.636747865890626	58.671441360787824	498.7072515666965	Ver
2	0.8822021484375	0.9050750732421875	0.0228729248046875	0.09877384224678078	2.489650349899085	8.636747865890626	43.71981320880587	480.91794529686456	Ver
3	1.6119537353515625	1.6456298828125	0.0336761474609375	0.0030423890660533033	0.06714686653334759	0.18068510179687503	29.694608065246943	1440.1884911644768	Ver
4	2.6720428466796875	2.7499847412109375	0.07794189453125	0.0057415059601836 21	0.05259794273394932	0.14732785223437503	12.830070477682067	2982.9913860610804	Ver
5	4.45703125	4.4847259521484375	0.0276947021484375	0.00250201003846228 14	0.050205037836369225	0.18068510179687503	36.10798898071625	6011.980165289257	Ver
6	6.858856201171875	6.9907684326171875	0.1319122314453125	0.01228397325219691	0.07517590737476552	0.18624464339062502	7.580798149219202	397.9919028340081	Ver

Figure 3 – Program GUI event visualization

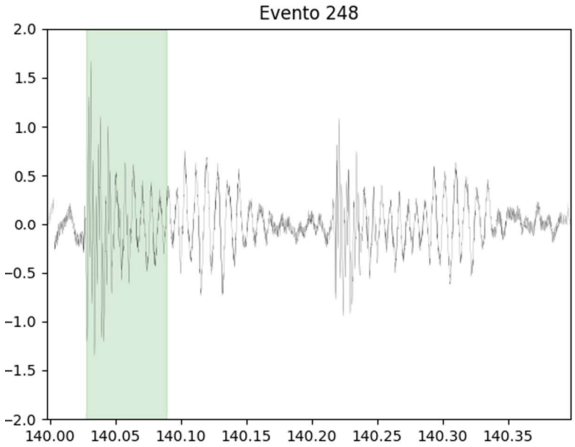

APPENDIX II – Reports generated

Figure 1 – CSV Report with data of each event

	A	B	C	D	E	F	G
1	Evento	Inicio	Fim	Duracao	En RILEM	En RMS	Amplitude
2							
3	1	3.346939	3.491425	0.144485	63989.73	229081.3	885760
4	2	5.023911	5.029678	0.005768	2902.184	606208	1006336
5	3	10.32022	10.47916	0.158936	72057.56	266624.5	906752
6	4	14.29207	14.51016	0.218094	79923.55	190539.4	732928
7	5	21.70943	21.74423	0.034805	17370.35	354109.3	998144
8	6	23.20035	23.3219	0.121552	45680.03	245306	751616
9	7	25.73535	25.82744	0.092087	41938.54	292918.1	910848
10	8	27.43794	27.50238	0.064438	28529.99	291128.9	885504

Figure 2 – Two examples of PDF pages, each with one event plotted